

Evolution of a stratified turbulent cloud under rotation

Tianyi Li^{1,2} †, Minping Wan^{1,3} ‡ and Shiyi Chen^{1,2,3} ¶

¹Guangdong Provincial Key Laboratory of Turbulence Research and Applications, Department of Mechanics and Aerospace Engineering, Southern University of Science and Technology, Shenzhen 518055, China

²State Key Laboratory for Turbulence and Complex Systems, College of Engineering, Peking University, Beijing 100871, China

³Guangdong-Hong Kong-Macao Joint Laboratory for Data-Driven Fluid Mechanics and Engineering Applications, Southern University of Science and Technology, Shenzhen 518055, China

(Received xx; revised xx; accepted xx)

Localized turbulence is prevalent in many geophysical flows where rotation and stratification are common features. Here we investigate the evolution of a stratified turbulent cloud under rotation. Since the turbulent cloud consists of vortices with different shapes and sizes, a single eddy under rotation and stratification is considered first. The stratified eddy is different from an eddy under pure rotation in two respects. First, a new potential vorticity (PV) mode is found, which is manifested as a static stable vortex. Second, inertial waves found in the purely rotating case are replaced by inertial-gravity waves in the stratified case. We then investigate a turbulent cloud for which we perform numerical simulations at a fixed Rossby number and for various Froude numbers. Unlike the purely rotating case where vertical columnar structures spontaneously grow out of the turbulent cloud, in the stratified case the columnar structures emerge and tilt away from the vertical direction. As the stratification gets stronger, the tilting angle increases and the rate of cloud expansion decreases. The columnar structures are composed of inertial-gravity waves, as both the tilting angles of the flow structures and vertical growth rates of the turbulent cloud can be predicted by the linear theory. We adopt Lagrangian particle tracking to identify regions dominated by wave and turbulence. When the stratification is weak, the inertial-gravity waves carry a considerable portion of energy away from the turbulent cloud. This portion of energy reduces as the stratification becomes stronger.

Key words:

1. Introduction

Localized regions of turbulence frequently take place in atmospheric and oceanic flows, where stable density stratification and rotation of the earth play important roles (Grant *et al.* 1968; Nasmyth 1970; Wijesekera & Dillon 1991; Nash *et al.* 2007; Yang *et al.* 2021). Therefore, investigating the evolution of turbulent patches under rotation and stratification is important for the understanding of many geophysical phenomena. In the

† Currently affiliation: Dep. of Phys. and INFN, Univ. of Rome “Tor Vergata”

‡ Email address for correspondence: wanmp@sustech.edu.cn

¶ Email address for correspondence: chensy@sustech.edu.cn

present study, we consider a horizontal turbulent cloud in a vertically stably stratified fluid with system rotation. We focus on the formation of flow structures with the relevant energy dispersion.

Many studies of the turbulence patch under rotation show that during the evolution of the system, there is a formation of columnar vortices parallel to the axis of rotation, which is relevant to the inertial waves (Hopfinger *et al.* 1982; Dickinson & Long 1983; Davidson *et al.* 2006; Ranjan & Davidson 2014). Dickinson & Long (1983) performed experiments of the oscillating-grid turbulence under the system rotation. When the Rossby number is of order unity, the front between disturbed and undisturbed fluid propagates at a speed proportional to the group velocity of zero-frequency waves in the direction of rotation axis. Davidson *et al.* (2006) conducted similar experiments where they oscillated the grid just once to generate a turbulent cloud and then investigated its following free evolution. They tracked the leading edge of the columnar structures and confirmed that its speed is proportional to the group velocity of inertial waves, suggesting that linear mechanisms are important for the formation of columnar vortices. Ranjan & Davidson (2014) carried out direct numerical simulations (DNS) of a turbulent cloud under different rotation rates. Columnar energy structures emerging from the cloud were observed and confirmed to be formed by inertial waves. Quantitative results showed that a large amount of energy of the localized turbulence can be carried away by the inertial waves, which play an important role in the energy dispersion.

The evolution of a localized turbulent region in a stratified fluid was also investigated in many researches, where radiation of internal waves from the turbulent patch is often observed (Thorpe 1982; Browand *et al.* 1987; De Silva & Fernando 1992, 1998). Intrusions are formed as the turbulent bulges in the lateral front become elongated horizontally (Browand *et al.* 1987). Manins (1976) illustrated that there exists zero-frequency columnar waves ahead of intrusions through a simplified hydraulic intrusion model. Maffioli *et al.* (2014) investigated the evolution of a stratified turbulent cloud using experiments as well as numerical simulations. The large-scale pancake-like structures emerging from the turbulent cloud are confirmed to be internal gravity wave-packets. A significant amount of kinetic energy is carried out of the turbulent cloud by the internal gravity waves, suggesting that the radiation of internal waves is an efficient mechanism of energy reorganization in the atmosphere and oceans.

Anisotropic structures and inertial wave propagation exist in both rotating and stratified turbulent flows, indicating close analogies between rotation and stratification (Veronis 1970; Maffioli *et al.* 2014), which are both important in many geophysical flows. The turbulent patch in a rotating stratified fluid was studied in many researches (Davies *et al.* 1991; Folkard *et al.* 1997; Wells & Helfrich 2004). Davies *et al.* (1991) generated a horizontal turbulent mixed layer and showed that the thickness of the mixed layer increases when the buoyancy frequency decreases. Ranjan & Davidson (2016) conducted DNS to study a horizontal buoyant turbulent cloud under rapid rotation. The rotation is vertical and the gravity is horizontal, as is the situation at the equator. It is confirmed that the formation of columnar structures is attributed to inertial waves arising from the buoyant cloud.

However, the evolution of a horizontal turbulent cloud under vertical rotation and stratification is also very relevant to many phenomena in geophysical flows, such as the atmosphere and oceans at high latitudes (Emery *et al.* 1984) and deep waters of the Arctic Ocean (Jones *et al.* 1995; Woodgate *et al.* 2001). Therefore, we study such case in the present paper and try to answer the following three questions. First, compared with the purely rotating case, how does the stratification change the flow structures emerging from the turbulent cloud? Second, are those flow structures formed by the inertial-gravity

waves and how do these flow structures change with the stratification? Third, how much energy of the cloud is carried away by the waves under different stratification?

2. The evolution of a single stratified eddy under rotation

In this section, we study the evolution of a single stratified eddy under rotation. This is motivated by the fact that a turbulent cloud can be considered as a sea of randomly oriented vortex blobs with different scales. Firstly, we introduce internal-inertial gravity waves under the Boussinesq approximation. Secondly, we analytically solve the initial value problem of a compact vortex blob in a rapidly rotating stratified environment. Finally, a numerical simulation is conducted to validate the analytical solution. It is shown that as the eddy evolves, a part of the energy is kept in the eddy by the PV mode while the other part disperses from the eddy by inertial-gravity waves.

2.1. Internal-inertial gravity waves

The Boussinesq set of equations for a linearly stratified fluid under system rotation can be written as:

$$\nabla \cdot \mathbf{u} = 0, \quad (2.1)$$

$$\frac{\partial \mathbf{u}}{\partial t} + \mathbf{u} \cdot \nabla \mathbf{u} = -\frac{1}{\rho_0} \nabla p + 2\mathbf{u} \times \boldsymbol{\Omega} - N\phi \mathbf{e}_z + \nu \nabla^2 \mathbf{u}, \quad (2.2)$$

$$\frac{\partial \phi}{\partial t} + \mathbf{u} \cdot \nabla \phi = Nu_z + \kappa \nabla^2 \phi, \quad (2.3)$$

where \mathbf{u} is the velocity vector, u_z is the z -component of the velocity, p is the modified pressure incorporating a centrifugal term, $\boldsymbol{\Omega} = \Omega \mathbf{e}_z$ represents the rotation vector, N is the Brunt-Väisälä frequency and ν and κ represents the kinematic viscosity and the diffusion coefficient, respectively. We define $\phi = (g/\rho_0 N) \rho'$, which has the dimension of velocity, and ρ' is the density perturbation from the ambient density.

Inertial-gravity waves can be obtained after a linearization of the Boussinesq equations. Neglecting molecular diffusion and the second-order terms of \mathbf{u} , \mathbf{w} , and ϕ , one obtains:

$$\frac{\partial \boldsymbol{\omega}}{\partial t} + \nabla \times (2\boldsymbol{\Omega} \times \mathbf{u}) = -N \nabla \phi \times \mathbf{e}_z, \quad (2.4)$$

$$\frac{\partial \phi}{\partial t} = Nu_z, \quad (2.5)$$

from which one finds (see Lesieur 1987, p. 56)

$$\frac{\partial^2}{\partial t^2} \nabla^2 u_z + 4\Omega^2 \frac{\partial^2 u_z}{\partial z^2} + N^2 \left(\frac{\partial^2 u_z}{\partial x^2} + \frac{\partial^2 u_z}{\partial y^2} \right) = 0. \quad (2.6)$$

This equation admits inertial-gravity waves with the dispersion relation given as

$$\varpi = \pm \sqrt{N^2 k_h^2 + 4\Omega^2 k_z^2} / k, \quad (2.7)$$

where ϖ is the frequency, while $k_h = \sqrt{k_x^2 + k_y^2}$ and $k = \sqrt{k_x^2 + k_y^2 + k_z^2}$ are the horizontal wavenumber and the total wavenumber, respectively. The group velocity is $\mathbf{c}_g = \nabla \varpi$, whose z -component is

$$c_{g,z} = \frac{\partial \varpi}{\partial k_z} = \pm \frac{(4\Omega^2 - N^2) k_h^2 k_z}{\sqrt{N^2 k_h^2 + 4\Omega^2 k_z^2} k^3}. \quad (2.8)$$

2.2. Analytical analysis of a single eddy

Following Davidson *et al.* (2006), we consider the evolution of an eddy in a stratified fluid under rotation and the process is assumed to be axisymmetric. In a cylindrical coordinate system (r, θ, z) , an axisymmetric velocity field \mathbf{u} can be divided into azimuthal and poloidal components

$$\mathbf{u} = (\Gamma/r) \mathbf{e}_\theta + \nabla \times [(\psi/r) \mathbf{e}_\theta], \quad (2.9)$$

where $\Gamma = u_\theta r$ is the angular momentum and ψ is the Stokes streamfunction. We substitute equation (2.9) into the linearized inviscid vorticity equation (2.4) and the linearized non-diffusive equation (2.5) to obtain

$$\frac{\partial \Gamma}{\partial t} = 2\Omega \frac{\partial \psi}{\partial z}, \quad \frac{\partial}{\partial t} (r\omega_\theta) = 2\Omega \frac{\partial \Gamma}{\partial z} + Nr \frac{\partial \phi}{\partial r}, \quad \frac{\partial \phi}{\partial t} = \frac{N}{r} \frac{\partial \psi}{\partial r}, \quad (2.10)$$

where $\nabla_*^2 \psi = (r\partial/\partial r)(r^{-1}\partial\psi/\partial r) + \partial^2\psi/\partial z^2 = -r\omega_\theta$, ∇_*^2 being the Stokes operator. Combining the equations in (2.10) yields

$$\frac{\partial}{\partial t} \left(\frac{\partial^2}{\partial t^2} \nabla_*^2 \Gamma + \left[(2\Omega)^2 \frac{\partial^2}{\partial z^2} + N^2 \left(r \frac{\partial}{\partial r} \right) \left(\frac{\partial}{r \partial r} \right) \right] \Gamma \right) = 0. \quad (2.11)$$

Equation (2.11) can be readily solved by using the Hankel-cosine transform

$$\hat{u}_\theta = \frac{1}{2\pi^2} \int_0^\infty \int_0^\infty r u_\theta J_1(k_r r) \cos(k_z z) dr dz, \quad (2.12)$$

where J_1 is the Bessel function of the first kind of order 1 and k_r and k_z are the wavenumbers in the r -direction and the z -direction, respectively ($0 \leq k_r, k_z < \infty$). Using the initial conditions $\hat{u}_\theta = \hat{u}_\theta^{(0)}$, $\psi = 0$ and $\phi = 0$, we have

$$\hat{u}_\theta = \left[\hat{u}_\theta^{(0)} / \left(N^2 k_r^2 + (2\Omega)^2 k_z^2 \right) \right] \left[N^2 k_r^2 + (2\Omega)^2 k_z^2 \cos \left(\sqrt{N^2 k_r^2 + (2\Omega)^2 k_z^2} t/k \right) \right], \quad (2.13)$$

from which we obtain

$$\begin{aligned} u_\theta = & 4\pi \int_0^\infty \int_0^\infty k_r \left[N^2 k_r^2 \hat{u}_\theta^{(0)} / \left(N^2 k_r^2 + (2\Omega)^2 k_z^2 \right) \right] J_1(k_r r) \cos(k_z z) dk_r dk_z \\ & + 2\pi \int_0^\infty \int_0^\infty k_r \left[(2\Omega)^2 k_z^2 \hat{u}_\theta^{(0)} / \left(N^2 k_r^2 + (2\Omega)^2 k_z^2 \right) \right] J_1(k_r r) \left[\cos \left(k_z z \right. \right. \\ & \left. \left. - \sqrt{N^2 k_r^2 + (2\Omega)^2 k_z^2} t/k \right) + \cos \left(k_z z + \sqrt{N^2 k_r^2 + (2\Omega)^2 k_z^2} t/k \right) \right] dk_r dk_z. \end{aligned} \quad (2.14)$$

We note that for the cases without stratification, i.e. $N = 0$, equations (2.13) and (2.14) lead to the same results obtained in Davidson *et al.* (2006), where only the system rotation is considered. In equations (2.13) and (2.14), the existence of stratification not only introduces a time-invariant term, but also modifies the frequencies of the wave-like terms. Note that the phase velocities of the wave-like terms, $\pm \sqrt{N^2 k_r^2 + (2\Omega)^2 k_z^2} / k$, are

of the same form as those of the inertial-gravity waves (2.7) if we replace k_r by k_h . This thus indicates that the wave-like terms correspond to the inertial-gravity waves. For the rotating stratified flow in a periodic domain, Smith & Waleffe (2002) show that the linear eigenmodes consist of two inertial-gravity waves and one PV mode. Therefore, the time-invariant term should correspond to the PV mode with zero frequency. In §2.3, we show the flow structures corresponding to inertial-gravity waves and the PV mode and then explain their roles in the energy dispersion.

2.3. Numerical validation of the analytical results

To estimate the applicability of the analytical results in §2.2 and develop a better understanding of the evolution of a single eddy in the rotating stratified fluid, a simple initial velocity field of the Gaussian-eddy form is chosen:

$$\mathbf{u} = A r \exp\left(-\frac{r^2 + z^2}{\delta^2}\right) \mathbf{e}_\theta, \quad (2.15)$$

for which Davidson *et al.* (2006) have given an analytical solution when only the rotation is considered. In this equation, A is the characteristic angular rotation rate and δ is the characteristic size. The corresponding Rossby and Froude numbers are defined by $Ro = A/(2\Omega)$ and $Fr = A/N$, respectively. At $Ro = 0.02, Fr = 0.16$, the analytical solution for an eddy ($A = 0.422, \delta = 0.125$) can be obtained by substituting (2.15) into (2.14).

A DNS of the evolution of this Gaussian eddy is also conducted. Equations (2.1)-(2.3) are solved using a parallelized pseudo-spectral code in a 512^3 periodic box of size $l_{box} = 2\pi$ and the fourth-order Runge-Kutta time-stepping scheme is adopted. The linear terms caused by rotation and stratification, along with viscous and diffusive terms, are integrated exactly by using an integrating factor technique. A combination of phase-shifting and truncation is used for de-aliasing of nonlinear terms (see e.g. Canuto *et al.* 2012). Figures 1(a) and (b) show u_θ^2 (normalized by its maximum value) contours in the $x-z$ plane passing through the axis of the Gaussian eddy at $t/t_f = 13.5$, obtained from the analytical solution and the DNS, respectively. Here, $t_f = 1/(2\Omega)$ represents the time scale of rotation. The DNS result closely resembles the analytical one, even though the DNS includes the viscous dissipation effects, which are absent in the analytical solution. It is notable that there is an intense area of u_θ^2 near the origin, which does not exist in the unstratified case (Ranjan & Davidson 2016, figure 3). This area is a physical manifestation of the PV mode, while the other intense areas correspond to inertial-gravity waves.

To illustrate the evolution of flow structures and the corresponding energy dispersion, figure 2 shows the iso-surfaces of the vertical vorticity, $\omega_z = 0.05$, color-coded with ϕ at $t/t_f = 13.5$ and 16.9. As the system starts to evolve, one vortex stays at the origin and two vortices are formed above and below it (figure 2(a)). At later times, the vortex near the origin changes slightly while the other two become very small with their centres being further away from the origin (figure 2(b)). This scenario is totally different from that in the purely rotating case (Ranjan & Davidson 2016), where two columnar structures are formed, which move away from each other and grow longer with time. The evolution of flow structures can be explained by the force balance between Coriolis and buoyancy forces. In figure 2(a), all three cyclonic vortices ($w_z > 0$) are subject to the Coriolis force which stretches them horizontally. For the vortex near the origin, ϕ has negative values on the top and positive values at the bottom, thus it is stretched vertically by the buoyancy force, which balances the Coriolis force since the fluid is incompressible. Therefore, this vortex is relatively stable and keeps the corresponding energy distribution

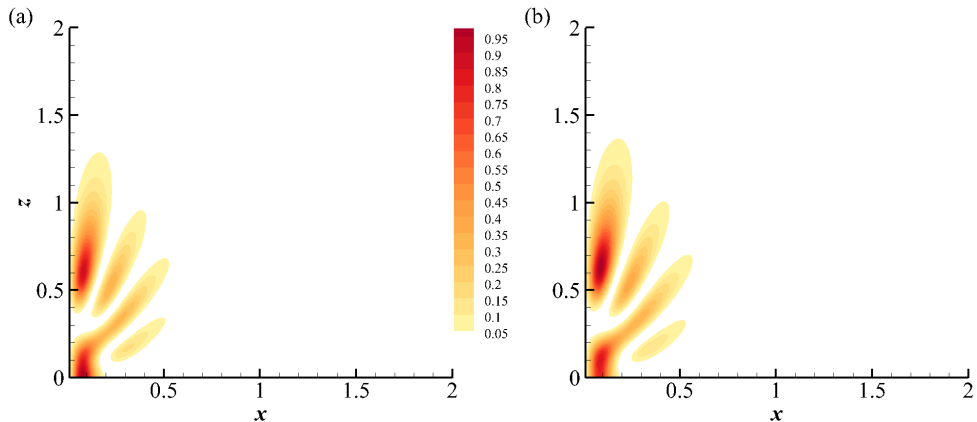


FIGURE 1. Contours of $u_\theta^2 / (u_\theta^2)_{max}$ in the $x-z$ plane passing through the axis of the Gaussian eddy, obtained from (a) analytical solution (2.14) and (b) the DNS, at $t/t_f = 13.5$.

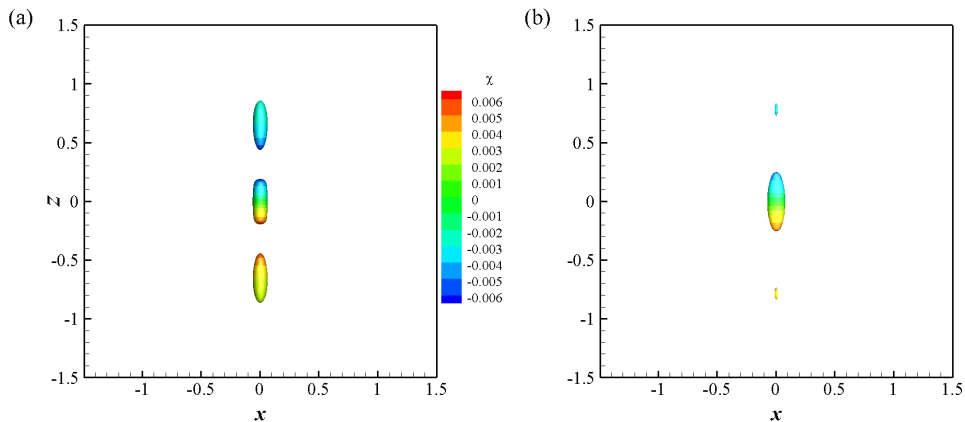


FIGURE 2. The iso-surfaces of $\omega_z = 0.05$ (front view) color-coded with ϕ obtained from the DNS at (a) $t/t_f = 13.5$ and (b) $t/t_f = 16.9$.

nearly time-invariant. For each of the other two vortices, ϕ does not change the sign and has larger absolute values for small $|z|$, indicating that the buoyancy force tends to push the vortex away from the origin and compress it vertically. Due to the combination of Coriolis force and buoyancy force, these two vortices move away and become smaller, which is associated with an energy dispersion and an exchange between potential and kinetic energies. Note that similar phenomenon as the vortex near the origin has been observed in homogeneous rotating stratified turbulence, where it is associated with the intense kinetic-potential energy exchange (Li *et al.* 2020a).

3. A stratified turbulent cloud under rotation

In this section, we move from a single eddy to the nonlinear evolution of a turbulent cloud. DNS are conducted to study the flow structures, which are then confirmed to be composed of inertial-gravity waves. At last, we calculated the amount of energy radiated

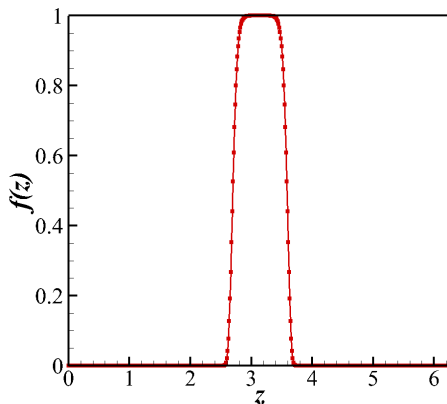


FIGURE 3. The spatial filter $f(z) = \exp(-10^a |z - \pi|^m)$ where $a = 4$ and $m = 9$.

from the turbulent cloud by inertial-gravity waves to quantify their importance in energy transfer for localized turbulent patches.

3.1. DNS of a turbulent cloud

Following similar procedure in Davidson (2015), DNS of fully developed homogeneous isotropic turbulence (HIT) was carried out to get the initial velocity field for the DNS of a turbulent cloud. A velocity field was then chosen at a time instant with an integral length scale $l_0 \approx 0.04l_{box}$ and a Reynolds number $Re_0 = u_0 l_0 / \nu \approx 176$, where u_0 represents the r.m.s. velocity. To numerically create a horizontal turbulent cloud, the velocity field from the HIT simulation was spatial-filtered by

$$f(z) = \exp(-10^a |z - \pi|^m), \quad (3.1)$$

which is shown in figure 3. Here we chose $a = 4$ and $m = 9$ in the simulations, which yields a thickness of the cloud $l_c = 0.13l_{box}$ that is about three times of the integral length scale l_0 . The buoyancy field was initialized with $\phi = 0$ throughout the domain. Therefore, the density profile was initially linear everywhere, indicating that no mixing had occurred within the cloud.

To investigate the effects of different stratification on the evolution of a turbulent cloud under rotation, DNS of a turbulent cloud were conducted at a fixed Rossby number, $Ro = 0.11$, and five different Froude numbers, $Fr = \infty$ ($N = 0$, the purely rotating case), 0.88, 0.44, 0.22 and 0.11. The simulation parameters of our DNS are tabulated in table 1, where $Ro = u_0 / (2\Omega l_0)$ and $Fr = u_0 / (Nl_0)$. Except the purely rotating case R0.11, simulations are named according to their Froude numbers, for instance, case F0.88 has a Froude number $Fr = 0.88$.

3.2. Evolution of flow structures

To display the evolution of the turbulent cloud structures, figure 4 shows iso-surfaces of u_z for all the simulations at different times. For the case R0.11 under pure rotation, figure 4(a) shows that vertical columnar structures emerge from the turbulent cloud and grow into the quiescent region, which is consistent with the previous experimental (Davidson *et al.* 2006) and numerical results (Ranjan & Davidson 2014). For the case F0.88, which has weak stratification, figure 4(b) shows that when compared to the case R0.11, the flow structures are only slightly different at $t/t_f = 8.4$ and moderately different at $t/t_f = 12.7$.

Case	Resolution	Ro	2Ω	Fr	N	l_c/l_{box}	l_c/l_0	ν	κ
R0.11	512^3	0.11	21.1	∞	0.0	0.13	3	0.001	0.001
F0.88	512^3	0.11	21.1	0.88	2.6	0.13	3	0.001	0.001
F0.44	512^3	0.11	21.1	0.44	5.3	0.13	3	0.001	0.001
F0.22	512^3	0.11	21.1	0.22	10.6	0.13	3	0.001	0.001
F0.11	512^3	0.11	21.1	0.11	21.1	0.13	3	0.001	0.001

TABLE 1. Simulation parameters for the DNS of a turbulent cloud.

For the cases F0.44 and F0.22 with stronger stratification, figures 4(c) and (d) show that the emerging columnar structures tilt away from the vertical direction as they grow into the quiescent region. In general, the angles between the columnar structures and the vertical direction are larger as the stratification gets stronger. Comparing figures 4(a)-(e), we find that at the same time instant, the vertical extent of the growing structures decreases as Fr gets smaller, indicating that the stable density stratification inhibits the expansion of the cloud in the vertical direction. This is consistent with the observations in the experiments of Davies *et al.* (1991).

The rotation frequency and the Brunt-Väisälä frequency are equal in the case F0.11 (figure 4(e)), where no structures grow out of the turbulent cloud, indicating that there is almost no energy radiated out of the cloud. This scenario is the same as that in the case without rotation and stratification (Ranjan & Davidson 2014). One possible explanation is that the stratification is strong enough to totally prevent the vertical expansion of the turbulent cloud under the system rotation. Note that equation (2.7) gives $\varpi = 2\Omega = N$ in this case, indicating that the frequencies of inertial-gravity waves are uniform in all directions. Therefore, the system is isotropic as there is no rotation and stratification.

3.3. Are the flow structures formed by inertial-gravity waves?

It is shown that columnar structures emerging from a turbulent cloud under rotation are formed by inertial waves (Ranjan & Davidson 2014) and large-scale pancake structures that grow out of a stratified turbulent cloud are internal gravity waves (Maffioli *et al.* 2014). In this section, we investigate whether the flow structures emerging from the stratified turbulent cloud under rotation are composed of inertial-gravity waves.

For all the simulations, the growth of flow structures in different directions results in the expansion of turbulent clouds in the vertical direction, which can be quantified through tracking the boundary of $|u_z|$ iso-surfaces with time. For example, given a threshold $|u_z^b|$, the upper and lower boundaries of the cloud can be obtained from the positions where $|u_z| = |u_z^b|$. Therefore, we can calculate the vertical extent of the cloud, $h(x, y, t)$, for each point on the x - y plane and time t . The mean wave-cloud thickness $\bar{h}(t)$ is defined as the average of $h(x, y, t)$ over x and y . Figure 5(a) shows the mean wave-cloud thickness for all the simulations where we choose $|u_z^b| = 0.22$. For the purely rotating case R0.11, the mean wave-cloud thickness shows a linear growth over time, which results from the inertial waves with $k_z = 0$ traveling at the group velocity $c_g = 2\Omega/k_h$ (Ranjan & Davidson 2014). For the case F0.88 with weak stratification, the mean wave-cloud thickness is close to that in the case R0.11 when $t \leq 0.2$, indicating that the stratification does not influence the cloud before $t = 0.2$. This is because that the linear time scale corresponding to the rotation, $t_f = 1/(2\Omega)$, is smaller than that corresponding to the stratification, $t_N = 1/N$. When $t > 0.2$, the mean wave-cloud thickness shows a smaller linear growth rate. For the cases F0.44 and F0.22 with stronger stratification, the behavior of the mean wave-cloud

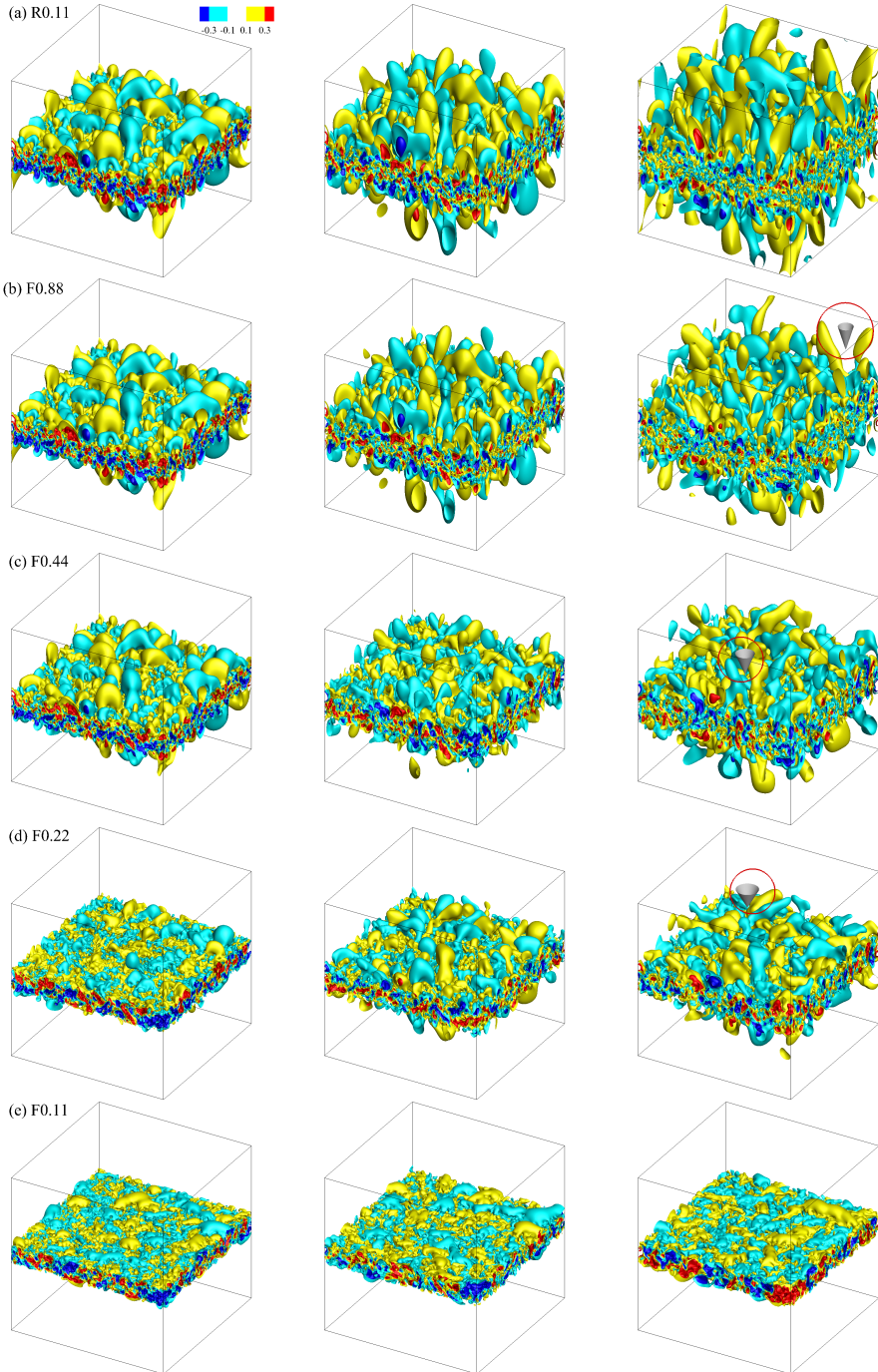


FIGURE 4. The evolution of iso-surfaces of u_z for the cases: (a) R0.11, (b) F0.88, (c) F0.44, (d) F0.22 and (e) F0.11 at $t/t_f = 4.2$ (left), 8.4 (middle) and 12.7 (right). Cones are plotted to indicate the predicted tilt angle of flow structures from the linear theory.

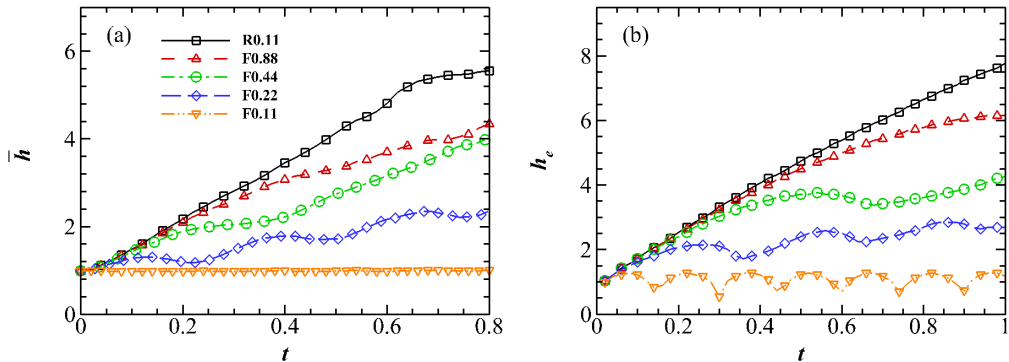


FIGURE 5. (a) The mean wave-cloud thickness \bar{h} of turbulent clouds in the simulations. (b) The vertical extent h_e of a Gaussian eddy evolving under the same Ro and Fr as those in the simulations.

thicknesses can be interpreted as the superposition of a linear growth and an oscillation with a fixed frequency over time. Moreover, the frequency is larger in the case F0.22. The mean wave-cloud thickness in the case F0.11 is almost constant with time, consistent with the observation in figure 4(e).

To investigate whether the flow structures are created by the superposition of inertial-gravity waves, we compare the results from the nonlinear simulations with those predicted by the linear theory. Since the initial turbulent cloud can be considered as a distribution of random vortex blobs of different shapes and sizes, we consider the linear evolution of a Gaussian eddy satisfying equation (2.15) under the same Rossby and Froude numbers. We set $\Lambda = 2.31$, $\delta = 0.125$ and $|u_z^b| = 5.5 \times 10^{-4}$ is used to determine the vertical extent of the eddy, h_e , which is the largest vertical distance between the positions where $|u_z| = |u_z^b|$. Figure 5(b) shows that the results of h_e are qualitatively consistent with those of \bar{h} in figure 5(a), indicating that the expansion of the turbulent cloud might be dominated by the linear mechanism.

Now we quantitatively illustrate that the flow structures are composed of inertial-gravity waves. For a vortex blob in the initial turbulent cloud, suppose that it is characterized by a length scale, $1/k$. Then its rescaled group velocity in the vertical direction is

$$\tilde{c}_{g,z} = kc_{g,z} = \pm \frac{2\Omega(1 - (N/(2\Omega))^2)(k_z/k_h)}{\sqrt{(N/(2\Omega))^2 + (k_z/k_h)^2(1 + (k_z/k_h)^2)}}. \quad (3.2)$$

Given the ratio of the Brunt-Väisälä frequency to the rotation frequency $N/(2\Omega)$, it is determined that when

$$\left(\frac{k_z}{k_h}\right)^2 = \frac{1}{4} \left[-(N/(2\Omega))^2 + \sqrt{(N/(2\Omega))^4 + 8(N/(2\Omega))^2} \right], \quad (3.3)$$

$\tilde{c}_{g,z}$ reaches the maximum $\tilde{c}_{g,z}^{max}$, which is the vertical growth rate of the turbulent cloud predicted by the linear inertial-gravity waves. Moreover, the corresponding value of $k_z/k_h = (k_z/k_h)_0$ characterizes the tilt angle of the flow structure. For the nonlinear simulations, the vertical growth rate of the turbulent cloud can be obtained from the growth rate of the mean wave-cloud thickness $\bar{h}(t)$ (figure 5(a)), which is calculated by a linear fitting method. Figure 6(a) shows the vertical growth rates of the turbulent cloud, α_{DNS} and α_{LT} , which are obtained from DNS and the linear theory, respectively. Both α_{DNS} and α_{LT} are normalized by their corresponding values when $N/2\Omega = 0$ for

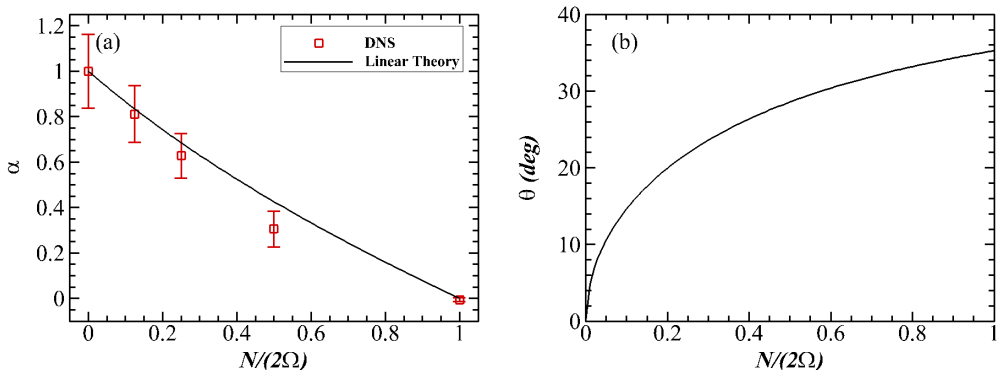


FIGURE 6. (a) Normalized vertical growth rates of the turbulent cloud, α , obtained from the DNS results and the linear theory. (b) The angle θ between the flow structure and the vertical direction predicted by the linear theory.

comparison. Figure 6(b) shows the angle between the flow structure and the vertical direction, $\theta = \arctan[(k_z/k_h)_0]$, which is predicted by the linear theory for different $N/(2\Omega)$. The results are consistent with figure 4, where the angle gets larger as $N/(2\Omega)$ increases. For quantitative comparison, we also plot cones in the third columns of figures 4(b), (c) and (d), where the angle between the conical surface and the vertical axis is equal to θ . It is notable that there is a good correspondence between the DNS results and the linear theory, although both α and θ are underestimated by the linear theory for the case F0.22, which is probably caused by the interaction between waves and turbulence since the vertical expansion of the cloud is small. Note that when both rotation and stratification exist, the frequency of the inertial-gravity waves (2.7) corresponding to $\tilde{c}_{g,z}^{max}$ is non-zero, which is the reason why there is an oscillation component of \bar{h} in the cases F0.44 and F0.22. The maximum group velocity always corresponds to the inertial (or gravity) waves with zero frequency when there exists only rotation (or stratification). In such case, methods such as two-dimensional energy spectrum analysis can be used to calculate the maximum group velocity, since the phase of u_z (Ranjan & Davidson 2014) or u_x (Maffioli *et al.* 2014) at the edge of the turbulent cloud would not change.

3.4. Wave-dominated and turbulence-dominated regions

In §3.3, it is shown that the flow structures emerged from the initial turbulent cloud are composed of inertial-gravity waves. To distinguish the regions dominated by waves and by turbulence, we use Lagrangian particle tracking to measure the vertical extent of the turbulence advection. Lagrangian particles are passive tracers whose position \mathbf{r} at time t satisfies that $d\mathbf{r}/dt = \mathbf{u}(\mathbf{r}, t)$. Here, \mathbf{u} is the fluid velocity and a 6th-order Lagrange interpolation is employed to find \mathbf{u} at the positions of the particles. A second-order Adams-Bashforth scheme is applied to integrate the positions of the particles. Tracer particles with a number $N_p = 65536$ are initialized randomly from a uniform distribution throughout the initial turbulent cloud, of which the vertical range is denoted as $[z_0, z_1]$. Let N_p^{out} be the number of particles outside of the range of the initial turbulent cloud. The r.m.s. distance of these particles to the initial turbulent cloud can be calculated as

$$d_{rms} = \sqrt{\frac{1}{N_p^{out}} \sum_{p=1}^{N_p^{out}} d_p^2}, \quad (3.4)$$

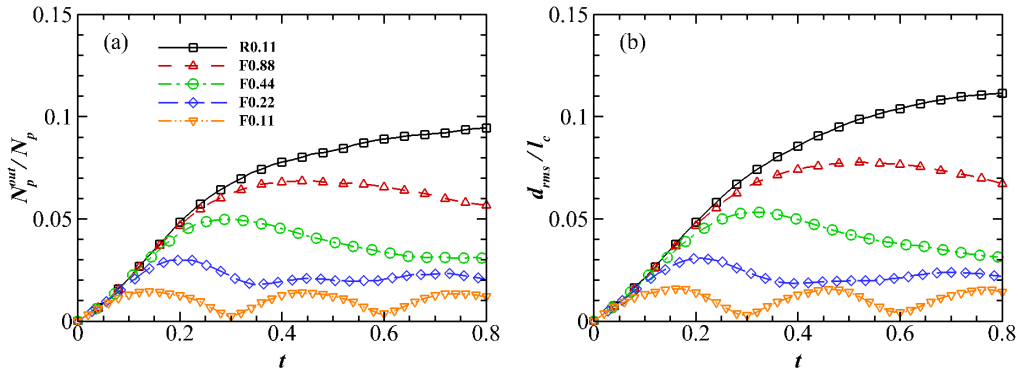


FIGURE 7. (a) The ratio of particles outside the initial turbulent cloud. (b) The r.m.s. distance of the outside particles to the initial turbulent cloud.

Case	R0.11	F0.88	F0.44	F0.22	F0.11
$\max(N_p^{out}/N_p)$	9.45%	6.86%	4.98%	2.99%	1.44%
$\max(d_{rms}/l_c)$	11.16%	7.77%	5.33%	3.08%	1.57%

TABLE 2. The maximum ratio of particles outside the initial turbulent cloud and the maximum vertical expansion of the initial turbulent cloud.

where

$$d_p = \begin{cases} z_p - z_1, & z_p > z_1 \\ z_0 - z_p, & z_p < z_0 \end{cases} \quad (3.5)$$

represents the distance of the particle p to the initial turbulent cloud. We consider $[z_0 - d_{rms}, z_1 + d_{rms}]$ as the vertical range of the turbulence-dominated region, and the other area is considered as the wave-dominated region. Figure 7 shows the ratio of particles outside the initial turbulent cloud, N_p^{out}/N_p , and d_{rms} normalized by the initial cloud thickness l_c . For the case R0.11, both N_p^{out}/N_p and d_{rms}/l_c increase with time, while for the cases F0.88 and F0.44, the two quantities first increase and then reduce after they reach the maximum values, which is probably caused by the stable stratification. However, both quantities reach stationary states around small values immediately in the cases F0.22 and F0.11, where the stratification is strong. Table 2 presents the maximum values of N_p^{out}/N_p and d_{rms}/l_c for all cases, where $\max(d_{rms}/l_c)$ can also be interpreted as the maximum vertical expansion of the initial turbulent cloud. It is observed that both quantities become smaller as the stratification gets stronger, indicating the restriction of vertical turbulent advection by stratification.

After regions dominated by waves and turbulence are identified, we can quantify how much energy of the turbulent cloud is carried away by the inertial-gravity waves, E^{wave} , which is the energy in the wave-dominated region. Figure 8(a) shows that for the cases where $Ro < Fr$, E^{wave}/E increases monotonically with time. Moreover, E^{wave}/E has smaller values as Fr decreases at a certain time, which indicates that the inertial-gravity waves contain less amount of energy under stronger stratification. For the case where $Ro = Fr$, E^{wave}/E oscillates at a fixed frequency with a nearly zero minimum and a maximum around 15%, showing that only at certain time a small amount of energy is carried out of the turbulent cloud by the inertial-gravity waves. Therefore, although the inertial waves take a considerable portion of energy when there only exists the system

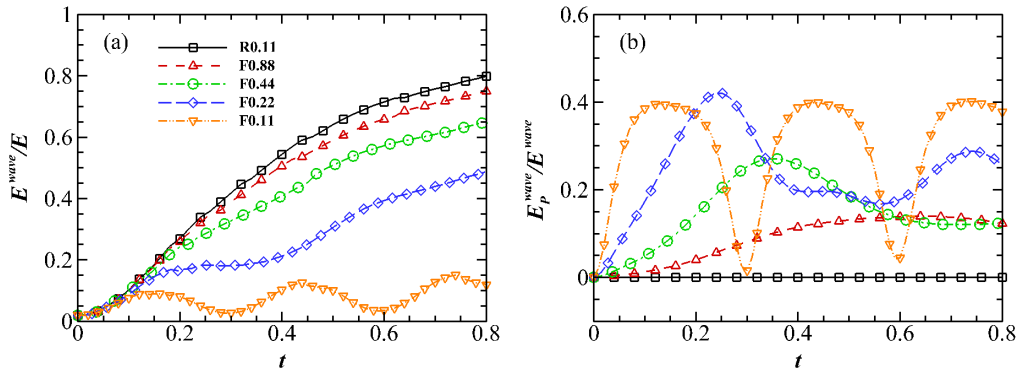


FIGURE 8. (a) The ratio of energy held in the inertial-gravity waves. (b) The ratio of potential energy to total energy in the wave-dominated region.

rotation, the amount of energy contained in the waves becomes less after the introduction of stratification. Figure 8(b) shows the ratio of potential energy to total energy in the wave-dominated region, E_P^{wave}/E^{wave} . As the stratification gets stronger, the potential energy plays an increasingly important role and changes more frequently with time. This indicates that the kinetic-potential energy exchange becomes increasingly important and the corresponding dominant inertial-gravity waves have larger phase velocities at higher stratification. Note that similar phenomenon of kinetic-potential energy exchange has been reported in homogeneous rotating stratified turbulence (Li *et al.* 2020b).

4. Conclusions and discussion

The evolution of a stratified turbulent cloud under rotation is studied in this paper. We first consider the evolution of a single eddy under rotation and stratification. Compared with the purely rotating case, two differences are found when the stratification exists. The first difference is that a new PV mode is identified, which takes the form of a stable vortex around the origin. Second, instead of the inertial waves found in the purely rotating case, there exist inertial-gravity waves with the dispersion relation depending on both rotation and stratification.

To study the nonlinear evolution of the turbulent cloud with different stratification under rotation, numerical simulations have been conducted. For cases where $Ro < Fr$, columnar structures spontaneously grow out of the turbulent cloud, which are vertical in the purely rotating case and tilt away from the vertical direction when the stratification is introduced. As Fr gets smaller, the tilt angle increases and the rate of cloud expansion decreases. For the system where $Ro = Fr$, no structures emerge from the turbulent cloud, which is similar as there is no rotation and stratification. We illustrated that the flow structures are composed of inertial-gravity waves as both DNS and linear theory give consistent results for the vertical growth rates of the turbulent cloud and for the tilt angles of the flow structures. Lagrangian particle tracking is used to distinguish regions dominated by wave and turbulence. It is shown that inertial-gravity waves emitted by the cloud could carry a significant portion of energy to the adjacent quiescent fluid and that the portion decreases as the stratification gets stronger. Therefore, inertial-gravity waves are crucial to the energy transfer in the atmosphere and oceans, where localized turbulent patches are often found.

The present study reveals some effects of stratification on the localized turbulence

under system rotation. First, compared with the purely rotating case, the existence of stratification introduces the zero-frequency PV mode, whose energy distribution barely changes with time. Second, the dominant inertial-gravity waves begin to tilt and have smaller vertical group velocity as the stratification becomes stronger. Both effects reduce the energy radiated outside the initial turbulent cloud. Note that in this study we have only considered the parameter regime where $Ro < Fr$. Although the regime of $Ro > Fr$ is thought to be more prevalent in the Earth's atmosphere and oceans (Riley & Lelong 2000), the regime of $Ro < Fr$ is relevant to many geophysical flows, such as in the deep sea where stratification is weak but rotational effects are dominant (Wingate *et al.* 2011; Heywood *et al.* 2002; Van Haren & Millot 2005; Timmermans *et al.* 2007, 2010). Moreover, the flow structures in the physical space can be considered as Fourier modes with phase coherence. Therefore, the evolution of turbulent clouds investigated in this study might also be interpreted as the evolution of the phase coherence of Fourier modes under rotation and stratification, which is worth investigating in the future.

Acknowledgements

This work has been supported by NSFC Basic Science Center Program (Grant No. 11988102) and NSFC Grant Nos. 91752201; Department of Science and Technology of Guangdong Province Grant No. 2019B21203001; Shenzhen Science and Technology Innovation Commission Grant No. KQTD20180411143441009; Key Special Project for Introduced Talents Team of Southern Marine Science and Engineering Guangdong Laboratory (Guangzhou) (GML2019ZD0103). Numerical simulations have been supported by Center for Computational Science and Engineering of Southern University of Science and Technology. T.L. thanks to Vikrant Gupta for proofreading the manuscript. M.W. acknowledges the support from Centers for Mechanical Engineering Research and Education at MIT and SUSTech.

Declaration of interests

The authors report no conflict of interest.

REFERENCES

- BROWAND, FK, GUYOMAR, D & YOON, S-C 1987 The behavior of a turbulent front in a stratified fluid: Experiments with an oscillating grid. *Journal of Geophysical Research: Oceans* **92** (C5), 5329–5341.
- CANUTO, CLAUDIO, HUSSAINI, M YOUSUFF, QUARTERONI, ALFIO, THOMAS JR, A & OTHERS 2012 *Spectral methods in fluid dynamics*. Springer Science & Business Media.
- DAVIDSON, PETER 2015 *Turbulence: an introduction for scientists and engineers*. Oxford University Press.
- DAVIDSON, PA, STAPLEHURST, PJ & DALZIEL, SB 2006 On the evolution of eddies in a rapidly rotating system. *Journal of Fluid Mechanics* **557**, 135–144.
- DAVIES, PETER A, FERNANDO, HARINDRA JS, BESLEY, PHILLIP & SIMPSON, RICHARD J 1991 Generation and spreading of a turbulent mixed layer in a rotating, stratified fluid. *Journal of Geophysical Research: Oceans* **96** (C7), 12567–12585.
- DE SILVA, IPD & FERNANDO, HJS 1992 Some aspects of mixing in a stratified turbulent patch. *Journal of Fluid Mechanics* **240**, 601–625.
- DE SILVA, IPD & FERNANDO, HARINDRA JS 1998 Experiments on collapsing turbulent regions in stratified fluids. *Journal of Fluid Mechanics* **358**, 29–60.
- DICKINSON, STUART C & LONG, ROBERT R 1983 Oscillating-grid turbulence including effects of rotation. *Journal of Fluid Mechanics* **126**, 315–333.

- EMERY, WJ, LEE, WG & MAGAARD, L 1984 Geographic and seasonal distributions of brunt-väisälä frequency and rossby radii in the north pacific and north atlantic. *J. Phys. Oceanogr* **14** (2), 294–317.
- FOLKARD, ANDREW M, DAVIES, PETER A & FERNANDO, HARINDRA JS 1997 Measurements in a turbulent patch in a rotating, linearly-stratified fluid. *Dynamics of atmospheres and oceans* **26** (1), 27–51.
- GRANT, HL, MOILLIET, A & VOGEL, WM 1968 Some observations of the occurrence of turbulence in and above the thermocline. *Journal of Fluid Mechanics* **34** (3), 443–448.
- HEYWOOD, KAREN J, GARABATO, ALBERTO C NAVEIRA & STEVENS, DAVID P 2002 High mixing rates in the abyssal southern ocean. *Nature* **415** (6875), 1011–1014.
- HOPFINGER, EJ, BROWAND, FK & GAGNE, Y 1982 Turbulence and waves in a rotating tank. *Journal of Fluid Mechanics* **125**, 505–534.
- JONES, EP, RUDELS, B & ANDERSON, LG 1995 Deep waters of the arctic ocean: origins and circulation. *Deep Sea Research Part I: Oceanographic Research Papers* **42** (5), 737–760.
- LESIEUR, MARCEL 1987 *Turbulence in fluids: stochastic and numerical modelling*. Nijhoff Boston, MA.
- LI, TIANYI, WAN, MINPING, WANG, JIANCHUN & CHEN, SHIYI 2020a Flow structures and kinetic-potential exchange in forced rotating stratified turbulence. *Physical Review Fluids* **5** (1), 014802.
- LI, TIANYI, WAN, MINPING, WANG, JIANCHUN & CHEN, SHIYI 2020b Spectral energy transfers and kinetic-potential energy exchange in rotating stratified turbulence. *Physical Review Fluids* **5** (12), 124804.
- MAFFIOLI, ANDREA, DAVIDSON, PA, DALZIEL, SB & SWAMINATHAN, NEDUNCHEZHIAN 2014 The evolution of a stratified turbulent cloud. *Journal of Fluid Mechanics* **739**, 229–253.
- MANINS, PC 1976 Intrusion into a stratified fluid. *Journal of fluid mechanics* **74** (3), 547–560.
- NASH, JD, ALFORD, MH, KUNZE, E, MARTINI, K & KELLY, SAM 2007 Hotspots of deep ocean mixing on the oregon continental slope. *Geophysical Research Letters* **34** (1).
- NASMYTH, PATRICK WALDEN 1970 Oceanic turbulence. PhD thesis, University of British Columbia.
- RANJAN, AVISHEK & DAVIDSON, PA 2014 Evolution of a turbulent cloud under rotation. *Journal of Fluid Mechanics* **756**, 488–509.
- RANJAN, AVISHEK & DAVIDSON, PA 2016 Dns of a buoyant turbulent cloud under rapid rotation. In *Advances in Computation, Modeling and Control of Transitional and Turbulent Flows*, pp. 452–460. World Scientific.
- RILEY, JAMES J & LELONG, MARIE-PASCALE 2000 Fluid motions in the presence of strong stable stratification. *Annual review of fluid mechanics* **32** (1), 613–657.
- SMITH, LESLIE M & WALEFFE, FABIAN 2002 Generation of slow large scales in forced rotating stratified turbulence. *Journal of Fluid Mechanics* **451**, 145–168.
- THORPE, SA 1982 On the layers produced by rapidly oscillating a vertical grid in a uniformly stratified fluid. *Journal of Fluid Mechanics* **124**, 391–409.
- TIMMERMANS, MARY-LOUISE, MELLING, H & RAINVILLE, LUC 2007 Dynamics in the deep canada basin, arctic ocean, inferred by thermistor chain time series. *Journal of physical oceanography* **37** (4), 1066–1076.
- TIMMERMANS, M-L, RAINVILLE, LUC, THOMAS, L & PROSHUTINSKY, ANDREY 2010 Moored observations of bottom-intensified motions in the deep canada basin, arctic ocean. *Journal of Marine Research* **68** (3-4), 625–641.
- VAN HAREN, HANS & MILLOT, CLAUDE 2005 Gyroscopic waves in the mediterranean sea. *Geophysical Research Letters* **32** (24).
- VERONIS, GEORGE 1970 The analogy between rotating and stratified fluids. *Annual Review of Fluid Mechanics* **2** (1), 37–66.
- WELLS, JUDITH R & HELFRICH, KARL R 2004 A laboratory study of localized boundary mixing in a rotating stratified fluid. *Journal of Fluid Mechanics* **516**, 83–113.
- WIJESEKERA, HEMANTHA W & DILLON, THOMAS M 1991 Internal waves and mixing in the upper equatorial pacific ocean. *Journal of Geophysical Research: Oceans* **96** (C4), 7115–7125.
- WINGATE, BETH A, EMBID, PEDRO, HOLMES-CERFON, MIRANDA & TAYLOR, MARK A 2011

- Low rossby limiting dynamics for stably stratified flow with finite froude number. *Journal of fluid mechanics* **676**, 546–571.
- WOODGATE, REBECCA A, AAGAARD, KNUT, MUENCH, ROBIN D, GUNN, JOHN, BJÖRK, GÖRAN, RUDELS, BERT, ROACH, AT & SCHAUER, URSULA 2001 The arctic ocean boundary current along the eurasian slope and the adjacent lomonosov ridge: Water mass properties, transports and transformations from moored instruments. *Deep Sea Research Part I: Oceanographic Research Papers* **48** (8), 1757–1792.
- YANG, CHU-FANG, CHI, WU-CHENG & VAN HAREN, HANS 2021 Deep-sea turbulence evolution observed by multiple closely spaced instruments. *Scientific Reports* **11** (1), 1–12.